Responses to anonymous referee #1:

We appreciate comments from this reviewer on our manuscript. Responses we made are below in red.

The paper presents terrestrial radar interferometry (TRI) measurements from Jakobshavn calving front. Three season of field measurements (measuring from 4 days to almost 2 weeks) of velocities and digital terrain models are presented. These radar data give new documentation/ verification the dynamics of the calving front. Physical challenges and dangers connected to field measurements in the calving area are well known, and this project is a valuable contribution to possible future development of measuring programs for increased knowledge of calving dynamics. The dynamic of the mélange in front of Jackobshavn calving front is one aspect that can make measurements demanding. The paper describes and discuss the calving cycle, with advance of the glacier front which forms a floating ice tongues during winter, and the retreat of the tongue by calving during summer.

The data set documents the grounding line migration during the calving season from velocities clearly modulated by tides (well presented in fig. 6), and thus the flotation of the calving front in a convincing way.

The paper is very well written, with clear language, relevant references, good method description and uncertainty discussions. It provides an interesting discussions of the dynamics of the melange on p. 6 , l.4 .

The data analysis is thoroughly, and the paper is well written. The paper clearly demon- strates the potential of radar monitoring of calving events, which is relevant due to expected increased in calving activity due to global warming with warmed oceans.

The only concern are the relevance of the very many figures, both in paper and supplementary text. It seems that the main figures are Fig 1, 2, 6, 9 and 13.

I suggest the authors consider removing all the other figures, and possibly try to simplify the figures they keep, and maybe combine differently and simplify the information here. The paper must then be slightly rewritten – where referring to the figures.

We have removed and combined some figures, the revised manuscript have 9 figures, and we have rewritten places where referring to the revised figures.

Specific comments: On p. 4, l. 1, Other errors in TRI data, such as phase variations associated with variable atmospheric water vapor, are difficult to model. Is this true? Corrections of refraction could be calculated from meteorological data if available?

In theory, if enough meteorological data were available, some corrections could be applied. However, in our case, it is difficult to do such corrections. There are two main reasons: 1) No well distributed stationary points are available to define a model, because we only have very limited near-field areas with targets that are not moving, and rocks points on the other side of the fjord have much lower coherence than the interested area. Points on ice can not be used to define a correction model because they are treated as kinematic targets. 2) Water vapor content varies significantly on space. During our campaigns, clouds or dense fog were sometimes seen in front of the ice cliff, but not other places. Besides, such errors should not change measured velocities significantly in the near-field, because the interferograms were formed between adjacent scans separated by 1.5-3 min. Phase variations due to changes of water vapor should be small in this short time span compared to the relatively large variations caused by fast ice motion. We therefore did not correct errors related with atmosphere. Instead, we analyzed data <10 km of the radar to minimize water vapor effects. In addition, we omitted data with SNR<1.5 in our tidal response analysis.

We have rewritten this sentence to state “Other errors in TRI data, such as phase variations associated with variable atmospheric water vapor between adjacent scans, are difficult to model but should not be significant in the nearfield given the 1.5–3 minute repeat time”.

Fig. 1, caption line 1, An intensity image.. (Specify: intensity of radar backscatter from your own measurements?)

Yes, this is an intensity image of radar backscatter from our measurement. We have added this information to the caption of Fig. 1 as “An intensity image of radar backscatter from the 2015 campaign (acquired 9 June 2015) is overlain on a Landsat-8 image (acquired 4 June 2015)”.

Fig. 2. Inserts in A,B,C, necessary info?

They were used to show a wider range of frequency, we have removed these inserts.

Fig. 3 – move to supplementary material?

Done.

Fig. 9 DEM from glacier front, derived from a one day average (please specify average of what)

This figure has now become Fig. 7. We have modified this sentence to “DEM for the glacier front, derived from median average of DEM estimates separated by 2 minutes during a 1 day period”.

Fig. 11. Necessary for readers of the Cryosphere? Quite simple principle.

This figure has now become Fig. 8. We think some readers may still be interested in it.

Fig. 13 and 14, combine to one figure?

Done. See Fig. 9.

Responses to anonymous referee #2:

We appreciate comments from this reviewer on our manuscript. Responses we made are below in red.

This study analyzed terrestrial radar interferometry data collected at Jakobshavn Isbrae during field campaigns in 2012, 2015, and 2016. Through tidal analysis of line-of-sight velocities, the authors conclude that the terminus is floating in early summer and becomes increasingly grounded as the terminus retreats throughout the summer. These observations build on previous work from Jakobshavn Isbrae and elsewhere, which together provide a consistent picture of terminus morphology. These observations pro- vide important insights into the processes influencing iceberg calving rates.

The observations in the paper are good, but the paper could use some editing to improve clarity and focus. For example, although interesting, the discussion of ice melange is not really relevant to the paper as written. I suggest either removing the discussion of ice melange or better integrating it into the text. The paper is about grounding line migration, but then there are some sentences and paragraphs about ice melange that are sprinkled throughout the manuscript but that don't really fit with the rest of the paper.

We have removed the discussion of ice melange that is beyond the scope of this paper.

The paper also isn't particularly long, which makes me wonder why additional text is needed in supplementary material. Couldn't it be incorporated into the manuscript? The portion about the feature tracking seems to be important, but is only briefly mentioned in the main text.

We have added a few sentences in the main manuscript to describe feature tracking method, please see Line 16-18 on page 4: “We compared this new velocity map with velocities estimated by feature tracking (done with Open Source Computer Vision Library: https://opencv.org/, uncertainty is typically <1 m d^{-1} for a pair of images separated by one day), which is independent of interferometry and does not require phase connection”. We also used RMS of velocities by feature tracking of stationary points to quantify the uncertainty, see the dashed white arc in Fig. 3(a) and the supplementary material.

Some of the figures could also use work: 1. The green lines in Figure 2 are almost undetectable, and the red and green lines will be difficult for some readers.

We have replaced the green lines with red lines. In our revised manuscript and supplement, we have tried to avoid using red and green for similar markers in the same figure.

2. Figure 6 is also really difficult to read, and it may be misleading in that the tidal response appears to grow in both the upglacier and downglacier directions, but is minimal somewhere in between. I understand that this is at least partially due to flow direction not corresponding with line of sight, but that needs to be made more clear. You could indicate that the smallest response occurs where the flow is perpendicular to line of sight.

The revised caption and manuscript should clarify the information in this figure (now Fig. 4).

Figure 4 (a, c, e) are used to show periodic variations, not long-term velocities. Apart from effects due to angles between flow directions and radar LOS, the observed velocity themselves

can have smaller amplitudes in between the upstream glacier and downstream glacier. This is especially true near the floating-grounding transition zone, where tidal responses on horizontal (out of phase with tides) and vertical (in phase with tides) directions can diminish each other, making the amplitude smaller.

It is not necessarily true that the smallest response occurs where the flow is perpendicular to line of sight. As we show in later discussion (e.g., Fig. 9 in the revised manuscript), the long-term LOS velocity can be the smallest (~0) when the flow is perpendicular to LOS, however, amplitude of the periodic signal is not necessarily the smallest here.

To make this figure more clear, we have also removed pink lines (glacier maximum/minimum extents) on (b, d, f).

3. Figure 9: It would be nice to see the location of the radar on these maps. Its pretty obvious where its located in the MLI images in previous figures, but not in the DEMs.

We have added a red dot in our revised manuscript to show the radar location (now Fig. 7).

4. Figure 12: I'm not sure what purpose this figure really serves.

The figure was used to assess the forcing due to surface melting. Maximum in the K1 tide rate occurs ~ 6 h after local noon. Assuming there is a diurnal signal caused by surface melting which could peaks ~6 h after local noon, it would be superimposed on the observed velocities. When observed from a positive LOS direction, this would enhance the diurnal signal; when observed

from a negative LOS direction, this would diminish the diurnal signal. This could explain why the diurnal component of power spectral density plot in Fig. 2(C) is smaller compared to boxes A and B.

We have removed this figure, and simplified our explanation into a few sentences in the first paragraph in section 4.2: "As shown in the normalized PSD in Fig. 2(C), the diurnal constituent is less obvious compared to Fig. 2(A, B): Assuming speed maxima caused by surface melting lags local noon by 6 h, it will be in phase with the K1 ocean tide rate. Due to the geometry difference, TRI-observed LOS diurnal tidal signal will be superimposed on a negative (box C) or positive (box A and B) diurnal signal associated with surface melting, decreasing or enhancing the observed signal. Thus the diurnal constituent in Fig. 2(C) is smaller compared to the other two areas".

5. Figure 13: Its really difficult to see the arrows in panel a. And why are feature tracking velocities projected onto line of sight? That seems backward and misleading to me, as it gives the impression that velocity variations are toward/away from the radar. I think it would be better to project the LOS velocities into map view, and then talk about what causes the variations in "true" velocity.

The figure has now become Fig. 9. In our revised manuscript. We show the 2-D velocity map from feature tracking in Fig. 3(a), and also show 2-D velocities for the other two campaigns in the supplement. However, in this figure, we show how the 2-D velocity would look in terms of radar LOS in order to explain to non-radar specialists some of the subtleties inherent in this imaging technique.

We projected feature tracking velocities onto LOS because we are trying to show points with velocities that are perpendicular to the radar LOS. As shown in the figure, the transition zone between dark red arrows and dark blue arrows match well with white areas on the LOS velocity map, indicating real velocities that are perpendicular to the radar LOS direction. We could plot these arrows using real velocities, however, the arrows would then not directly linked to the phase derived LOS velocities. We therefor believe it is better to project velocities onto LOS for this figure, and readers who read the caption hopefully will not misunderstand the figure.

We have changed the arrow colors to dark red (towards the radar) and dark blue (away from the radar) to allow better visibility.

Some specific comments: Page 1, Line 5: I would not say that ice is locally thin if the freeboard is less than 125 m!

We have changed it to “much thinner compare to ice >1 km upstream”.

Page 1, Line 22: “down dipping upstream bed” is confusing. Do you mean retrograde bed?

Yes and we have adopted the referee’s suggestion using “retrograde”.

Page 2, Line 2: “ice speed accelerates” – speed doesn’t accelerate, but ice does

We have removed “speed”.

Page 2, Line 15: “grounding line position” is not really a “basal condition”

This now becomes Line 14 on Page 2. We have rewritten this sentences to “Currently, it is challenging to observe grounding line position directly when it lies near the calving front”.

Page 2, Line 30: “through a calving season”? This makes it sound like you were operating the TRI all summer long, which is misleading.

This now becomes Line 28-30 on Page 2. We have rewritten this sentence to “Here we use TRI measurements obtained in three summer campaigns, but at different stages (early versus late summer) of the calving season, to investigate tidal response and the evolving glacier front through Jakobshavn Isbræ’s calving season”.

Page 5, Line 19: “The amplitude” of? I’m not quite sure what this refers to.

This now becomes Line 21-22 on Page 5. We have changed this sentence to “The amplitude of variation is magnified by frequency”. Please see Supplementary Text S3 for detail.

Pages 5-6 (and supplement): The step-change in ice melange thickness is interesting and suggests that the ice melange has a “terminus”. However the discussion is highly speculative and doesn’t really fit in this subsection, which is about tidal analysis. Also, I don’t buy the idea that the change occurs because of some bedrock topographic feature. I wonder if instead you are seeing the remnants of the winter melange that hasn’t yet lost cohesiveness.

We have removed this discussion about the melange. The thick melange is not likely to be the remnants of the winter melange since we see some large calving events from Landsat-8 and Sentinel-2 satellite images earlier in the spring. Those calving events should have removed pro-glacial melange accumulated in winter, although re-freezing is possible. Another possibility is the instead of bedrock obstructions, the obstructions are on the sides of the fjord, ie the fjord near this point and occasionally becomes choked with ice.

Page 7, Lines 19-20: This seems like a pretty big assumption, considering that other studies have suggested year-to-year variability in tidal response.

This has now become the first paragraph on Page 7. We acknowledge that year-to-year variability in tidal response is possible. However, position time series of the calving front derived from satellite images supports this assumption. As shown in Fig. 5, Jakobshavn Isbræ had a relatively regular advance and retreat over the five year observation period. Joughin et al. (2008, 2014) documented strong seasonality in speed that shows a good inverse correlation with the seasonally varying length of a short ice tongue. In addition, our 2015 and 2016 data provide a comparison of tidal responses both in early summer but from different years, they have similar behavior. There is also similarity between our 2012 campaign and Podrasky et al (2014) in late summer but in different years. For these reasons, we assume a regular variation in tidal response over the 5 five year spanning our observation period.

We have added a few more sentences to the first paragraph on Page 7 to support this assumption.

Page 8, equation 3: Double check this equation. I'm pretty sure that V_los and dh/dt should be swapped.

We apologize for the confusion, we are grateful that the referee pointed out some questions on this equation. H_0 is the mean height difference between the radar and the target, not "the mean height of the target" as we wrote in our previous draft. And V_{los} represents the TRI-observed LOS velocity (not "vertical" as in our previous draft). We have corrected this. Apart from that, the equation remains unchanged. The figure below shows these relations, where blue dot represents the radar, red square shows the mean vertical position of the target, red dot is the vertical position at current time, other parameters are the same as described in the manuscript. We have added this figure to the supplement.

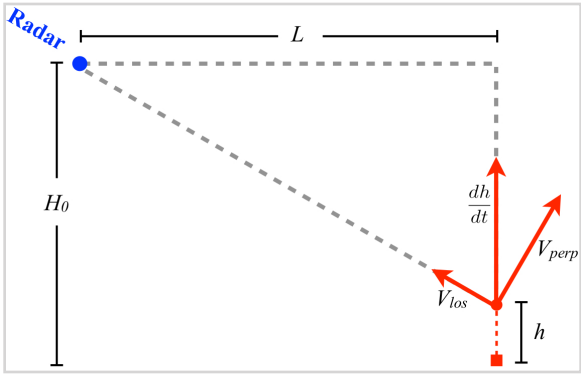

Page 8, Line 17: dh/dt ~ 0.1*tidal rate in the melange due to buoyancy effects, and less than that for the glacier.

This is in Line 7 on Page 8 now. Please see our response to the previous comment. As dh/dt denotes vertical component of ice velocity, it is approximately equal to tide rate in the melange. We have added the phrase "and less than that for the glacier".

Grounding line migration through the calving season ~~of~~ at Jakobshavn Isbræ, Greenland, observed with terrestrial radar interferometry

Surui Xie[1], Timothy H. Dixon[1], Denis Voytenko[2], Fanghui Deng[1], and David M. Holland[2,3]

[1]School of Geosciences, University of South Florida, Tampa, FL, USA
[2]Courant Institute of Mathematical Sciences, New York University, New York, NY, USA
[3]Center for Global Sea Level Change, New York University, Abu Dhabi, UAE

Correspondence to: Surui Xie (suruixie@mail.usf.edu)

Abstract.

Ice velocity variations near the terminus of Jakobshavn Isbræ, Greenland were observed with a terrestrial radar interferometer (TRI) during three summer campaigns in 2012, 2015, and 2016. ~~Ice velocity variations appear to be largely modulated by ocean tides.~~ We estimate a ∼1 km wide floating zone near the calving front in early summer of 2015 and 2016, where ice moves in phase with ocean tides. Digital Elevation Models (DEMs) generated by the TRI show that the glacier front here ~~is thin~~ was much thinner (ice surface ~~is~~ <125 m above local ~~water level)~~ sea level) compare to ice >1 km upstream. However, in late summer 2012, there is no evidence of a floating ice tongue in the TRI observations. Ice surface elevation near the glacier front was also higher, >140 m above local sea level within a very short distance (<1 km) from the ice cliff. We hypothesize that during Jakobshavn Isbræ's recent calving seasons, the ice front advances ∼3 km from winter to spring, forming a >1 km floating ice tongue. During the subsequent calving season in mid- and late-summer, the glacier retreats by losing its floating portion through a sequence of ~~iceberg~~ calving events. By late summer, the entire glacier is likely grounded. In addition to ice velocity ~~variations driven by tide rise and fall~~variation driven by tides, we also observed a transverse velocity variation in the mélange and floating ice front. This across flow-line signal is in phase with the first time derivative of tidal height, and is likely associated with tidal currents or bed topography.

1 Introduction

Greenland's largest marine-terminating glacier, Jakobshavn Isbræ, has doubled in speed and retreated tens of km in the last few decades (Joughin et al., 2004; Rignot and Kanagaratnam, 2006; Joughin et al., 2008; Howat et al., 2011). This process has been attributed to several processes, including increased subsurface melting and iceberg calving triggered by relatively warm ocean water (Holland et al., 2008; Motyka et al., 2011; Enderlin and Howat, 2013; Myers and Ribergaard, 2013; Truffer and Motyka, 2016). In recent years, the glacier has maintained a relatively stable terminus position despite continued speedup, primarily due to the fact that the glacier is now embedded in the ice sheet, with large inflows of ice from the sides supplying ice to the main glacier channel, albeit with some thinning (Joughin et al., 2008). However, it is not clear if ~~the position and status are~~

this configuration is stable, as Jakobshavn Isbræ has a ~~down-dipping upstream~~ retrograde bed (Clarke and Echelmeyer, 1996; Gogineni et al., 2014). Some numerical models suggest that glaciers with reverse bed slopes cannot maintain stable grounding lines, as bed topography favors ingress of warm fjord bottom water, accelerating melting at the ice-ocean interface (e.g., Vieli et al., 2001; Schoof, 2007).

In addition to the dramatic secular speedup and retreat, there are strong seasonal variations in both ice speed and front position at Jakobshavn Isbræ. These have ~~a strong~~ an inverse correlation: ice ~~speed~~ accelerates through spring and summer but slows down in winter, while glacier front position retreats from spring to summer, reaching a minimum in late summer when ice speed is maximum (Joughin et al., 2008). This supports the hypothesis that loss of the buttressing ice tongue during the calving season contributes to Jakobshavn Isbræ's seasonal speedup. The rapid acceleration since 2000 may thus be the sequential result of losing its large floating ice tongue from 1998 to 2003 (Joughin et al., 2004, 2008), though Van Der Veen et al. (2011) suggested that progressive weakening of ice in the lateral shear margins is a more plausible explanation to the acceleration. By investigating interactions between the glacier and its ~~proglacial~~ pro-glacial ice mélange, Amundson et al. (2010) interpreted the seasonal advance and retreat of the glacier terminus as an effect of seasonally-variable rheology in the ice mélange: stiffened mélange in winter suppresses major calving events, enabling the terminus to move forward; while in summer, a weaker mélange can no longer prevent major iceberg calving, and the terminus retreats. They used a force balance analysis to demonstrate that large-scale (full-glacier-thickness icebergs) calving events are not likely to occur when the ice front is well-grounded. Based on this, they suggested that one of the necessary conditions for frequent full-glacier-thickness iceberg calving at Jakobshavn Isbræ is a floating or close-to-floating terminus in summer.

Currently, ~~there is no efficient approach to observe basal conditions of marine-terminating glaciers directly~~ it is challenging to observe grounding line position directly when it lies near the calving front. However, ~~some basal conditions, such as grounding line position,~~ this can be inferred from ~~measured~~ observations of ice motion (Heinert Riedel, 2007; Rignot et al., 2011; Rosenau et al., 2013). ~~It has been observed that for~~ For many marine-terminating glaciers, ice speed is affected by ocean tides (e.g., Makinson et al., 2012; Podrasky et al., 2014; Voytenko et al., 2015a). At Jakobshavn Isbræ, Podrasky et al. (2014) used GPS and theodolite data obtained in a two-week campaign in middle to late August 2009 to study velocity response to ocean tidal forcing near the terminus of Jakobshavn Isbræ. After removal of ~~large~~ a high background speed and ~~perturbation~~ perturbations caused by a single calving event, tidal forcing explained ~~10%–90%~~ a significant fraction of the remaining signal. Based on the fast decay of tidal ~~responses~~ response upstream, they concluded that the terminus region is very nearly grounded during summer months. Rosenau et al. (2013) used photogrammetric time-lapse imagery to estimate groundling line migration and calving dynamics at Jakobshavn Isbræ. They found that the groundling line retreated 3.5 km from 2004 to 2010, with an ephemeral floating tongue during the advance season.

In this study, we use ice velocity and elevation time series observed with terrestrial radar interferometry (TRI) to analyze groundling line position and tidally affected ice flow. Previous work (Peters et al., 2015; Voytenko et al., 2015a, b, c, 2017; Holland et al., 2016; Xie et al., 2016) has shown that TRI can overcome the limitations of GPS (low spatial resolution, difficult to deploy near the calving front), theodolite (low spatial resolution and precision), photogrammetry (low reliability in bad weather and at night), and satellite observations (low temporal resolution). Here we use TRI measurements obtained in three

summer campaigns, but at different stages (early versus late summer) of the calving season, to investigate tidal ~~responses~~ response and the evolving glacier front through ~~a~~ Jakobshavn Isbræ's calving season.

2 Data Acquisition

We observed the terminus of Jakobshavn Isbræ in three summer campaigns in 2012, 2015, and 2016. Each campaign obtained a continuous record of velocity and elevation change over 4 to 13 days. The TRI instrument is a real-aperture radar operating at Ku-band (1.74 cm wavelength) and is sensitive to line-of-sight (LOS) displacements of ∼1 mm (Werner et al., 2008). It has one transmitting and two receiving antennas, which allows for high spatial and temporal resolution measurements of both displacement and topography. The antennas are rigidly attached ~~with~~ to a rack structure, which sits on a motor that rotates around a fixed vertical axis. In 2012, the instrument was deployed on a tripod reinforced with sandbags, with the calving front ∼3–6 km away. In 2015 and 2016, the instrument was mounted on a metal pedestal ~~that was bolted ~~connected to bedrock with 10 cm ~~deep into solid rock~~bolts, and protected by a radome to eliminate disturbance from wind and rain, with the calving front ∼2–5 km away. In all three campaigns, the radar scanned to a maximum distance of 16.9 km, generating images with both phase and intensity information. The resolution of the range measurement is ∼1 m. The azimuth resolution varies linearly with distance, and ~~is determined by~~ varies as the arc length ~~$l = D \cdot A$, where D~~ , where $l = D \cdot A$, D is the distance to the radar, and ~~A~~ A is the azimuth angle step in radians. In all three campaigns, the azimuth angle steps were set to be 0.2°, resulting in an azimuth resolution of 7 m at 2 km distance, 14 m at 4 km, etc.. Other parameters in these measurements are listed in Table 1. Figure 1 shows the spatial coverage of measurements in each campaign.

3 Data analysis

3.1 TRI data processing

TRI data were processed following Voytenko et al. (2015b): 1) slant range complex images were multi-looked to reduce noise; 2) interferograms were generated between adjacent scans; 3) A stationary point on rock was chosen as reference for phase unwrapping. Unwrapped phases were then converted to line-of-sight (LOS) velocities. We define LOS velocity as positive when ice moves towards the radar, and negative when ice moves away from the radar. All results were resampled into 10 m × 10 m pixel spacing maps unless otherwise specified, with a bicubic spline interpolation algorithm. To georeference the TRI results, we used a Landsat-7/8 image acquired during (if not, <2 day time difference) the observation period as reference. By fixing the radar location and horizontally rotating the intensity image, a rotation angle was estimated based on the best match of distinct surface features (e.g., coast line, ice cliff, icebergs, etc.), thus TRI-derived results were georeferenced into the earth reference system. In this study, we ~~used~~ use the polar stereographic projection to minimize distortion. Notice that the TRI instrument measures LOS intensity and phase information. Converting LOS data into x-y grid coordinates induces some distortions due to topography, especially in the mélange close to the radar, where ~~height difference is the~~ the height differences are largest. The radar location in 2012 was ∼280 m above local ~~water~~ sea level, and in 2015/2016 ∼200 m above local ~~water~~

sea level. A simple calculation based on geometry shows that distortion due to topography is <15 m. There are two other error sources in georeferencing TRI data: 1) Radar position error (it was measured with a single frequency GPS, with location error estimated at less than 10 m); 2) Rotation error in matching TRI and Landsat images. By comparing georeferenced TRI images with different Landsat-7/8 images, we found no visible mismatch larger than 4 pixel ~~width~~ widths of the satellite images. We thus assess that the coordinate error in georeferenced TRI results is <60 m, i.e., smaller than 4 ~~pixel~~ pixels (typically <2 ~~pixel) width~~ pixels) of Landsat-7/8 panchromatic images. Moreover, because the radar was deployed on a fixed point ~~for each respective~~ in each campaign, and we used the same radar coordinates and rotation angle in georeferencing for each campaign, the error due to georeferencing will not affect our time series analysis. Other errors in TRI data, such as phase variations associated with variable atmospheric water vapor between adjacent scans, are difficult to model but should not be significant in the nearfield given the 1.5–3 minute repeat time. To minimize water vapor effects, we only analyzed data within 10 km of the radar unless otherwise specified.

TRI data obtained in 2015 have been previously discussed in Xie et al. (2016). The same data are used here, but we added 17 h of additional data obtained before the period analyzed by Xie et al. (2016). The additional data were acquired when the instrument was in an experimental mode: rather than 150° of scan, the scanned arc was sometimes set to different values, and the repeat time was sometimes 1 or 2 min rather than 1.5 min. Otherwise, the additional data have the same quality as ~~the~~ subsequent acquisitions. We processed the additional data with the same standards and converted it into the same reference frame as the remaining 2015 data.

Except for several rapid changes in velocity caused by calving events, the processed results from 2015 and 2016 ~~show~~ have good continuity. However, velocities from 2012 have some significant offsets (Supplementary Fig. S1(a)). Most of these offsets reflect phase unwrapping errors, reflecting ~~an~~ incorrect integer multiples of microwave cycles ~~has been~~ applied during the phase unwrapping process. The repeat time in 2012 (3 minutes) was longer than the other two years, and ice motion relative to ~~the~~ adjacent areas in the radar LOS during that interval could exceed 1 radar wavelength. We fixed ~~the~~ these phase offsets in 3 steps: 1) ~~Estimating~~ Estimate the velocity time series at a single point on the ice (with integer multiples of microwave cycles corrected); 2) ~~Using~~ Use this kinematic point as the reference point for phase unwrapping to get relative velocities for all other ~~points mapped~~ mapped points; 3) ~~Adding~~ Add the velocity model from step 1 to the relative velocities. We compared this new velocity map with velocities estimated by feature tracking ~~,~~ (done with Open Source Computer Vision Library: https://opencv.org/, uncertainty is typically <1 m d^{-1} for a pair of images separated by one day), which is independent of interferometry and does not require phase connection. The phase jumps are greatly reduced, and we believe the resulting velocity time series are an accurate indicator of ice motion. Details are given in ~~the~~ Supplementary Text S1.

3.2 Tidally driven ice motion analysis

The calving front is where the glacier directly interacts with the ocean. By changing back-pressure on this front, ocean tides are known to influence the behavior of some marine-terminating glaciers (Walters, 1989; Anandakrishnan and Alley, 1997; Podrasky et al., 2014). Besides back-pressure, a full-Stokes nonlinear viscoelastic model (Rosier and Gudmundsson, 2016) suggests that when there is a floating ice tongue, tidal flexural stress can also be an important forcing for marine-terminating

glaciers. In addition, tidal variation can influence basal friction at the ice-bed interface, thus changing the sliding rate of the glacier (e.g., Walker et al., 2013; Voytenko et al., 2015a).

For all three campaigns, velocities near the terminus show significant semi-diurnal variations, and perhaps a small diurnal signal. Figure 2 shows the power spectral density analysis (PSD) for selected data in 2016. PSDs for 2012 and 2015 are shown in the Supplementary Fig. S6 and S7. Previous studies indicate that apart from calving events, short-term ice velocity variations at Jakobshavn Isbræ are well described with simple tidal response models (e.g., Rosenau et al., 2013; Podrasky et al., 2014). Diurnal variation caused by surface melting may also contribute to velocity variation. This has been observed at both Jakobshavn Isbræ (Podrasky et al., 2012) and Helheim Glacier (Davis et al., 2014)~~)~~. Due to the short time span of our data, it is not possible to recover the full temporal spectrum of ice velocity variations. Instead, we focus on the largest spectral components of the velocity field.

There was no tide record in the fjord near the terminus during our campaigns. Podrasky et al. (2014) analyzed a 14 day tide record in the fjord within 5 km of the calving front obtained in August 2009, and compared it with a longer record from Ilulissat. The two datasets show close agreement, with no measurable delay in time, and a maximum difference in stage <10 cm. Thus they used the longer record of tides at Ilulissat to analyze the tidal response of the glacier. ~~Similarly, we~~ We also used analyzed tidal constituents from the long-term record at Ilulissat to predict ~~the~~ tides in the fjord during our campaigns. Richter et al. (2011) applied harmonic tidal analysis to 5 years of long-term sea-level records at Ilulissat and estimated that the largest 3 tidal constituents are K1, M2 and S2, with amplitudes of 0.331 m, 0.671 m and 0.273 m respectively. These three constituents account for >95% of all the ~~tidal constituents analyzed by Richter et al. (2011). Figure 3~~ analyzed tidal constituents. Supplementary Fig. S8 shows the predicted tide and tidal rate (defined as the *1*st time derivative of tidal height) during the 2015 campaign, when we had a mooring deployed at the mouth of the fjord (red hexagon in Fig. 1) that recorded tidal height. There are only small differences between measured tide or tidal rate with predictions using the three largest constituents. In the following analysis, we focused on ice velocities with the same frequencies as the K1, M2 and S2 tide constituents. Other components of tidal motion with similar frequencies will be aligned into these 3 constituents. For example, diurnal variation caused by surface melting with a period of ∼1 d, if it exists, will not be separable from K1 with a period of 1.0027 d.

Many tidal response models analyze the response of ice position to tidal height variation (e.g., Davis et al., 2014; Podrasky et al., 2014). However, our TRI ~~measurement is~~ measurements are only sensitive to LOS displacement. The corresponding velocity derived by interferometry is the *1*st time derivative of LOS displacement. Velocity can be converted to position by integration, however, due to data gaps and the nonlinear behavior of the velocity time series, integration of velocity time series may introduce artifacts. Therefore, we used ice velocity instead of position and analyzed the response of ice velocity to tidal rate. The amplitude ~~will be amplified~~ of variation is magnified by frequency (~~signal with a higher frequency will have a larger range~~ signals with higher frequencies will have larger ranges of *1*st time derivative~~, see~~ . See Supplementary Text S3), but the phase difference is unchanged by differentiation.

Before the tidal response analysis, we used the modified Z-score method (Iglewicz and Hoaglin, 1993, also see Text S1 in the Supplement) to remove outliers. We note that TRI-observed ice motion in the mélange is very sensitive to ~~even very~~ small calving events, while ice on the glacier is less ~~sensitive to small calving events~~affected. For the 2012 data, due to frequent

calving events, we were not able to ~~phase unwrap~~ accurately model the full time series. Instead, we used data obtained from 6 August to 10 August when there was only one small calving event (see Supplementary Fig. S1) for the following analysis. For the 2015 data, there were many small calving events and a large one at the end (Xie et al., 2016), ~~which resulted~~ resulting in a noisy time series for the mélange. We therefore omitted the 2015 mélange from further analysis. For 2016, a step-change in ice elevation (dashed purple line in Fig. 2~~, also marked by red arrow in Fig. 4~~) was observed, separating the mélange into two distinct parts. Downstream from the step-change, ice motion is very noisy and difficult to analyze for periodic ~~signal~~signals. Upstream from that, ice velocity variation is similar to the glacier. Therefore, we did not do tidal response analysis for the ice mélange downstream from the step-change ~~zone~~ in 2016. ~~Movie~~ Movies S1, S2, and S3 in the Supplement show all major calving ~~events observed during the three campaigns, and consequent changes in the mélange.~~

~~A comprehensive study of the step-change in the 2016 mélange is beyond the scope of this paper, but we note that many~~ or calving-like ~~events occurred near this front. Ice surface height upstream of the step-change is ~10 m higher than downstream from the step-change (see Supplementary Text S4 and Fig. S8(c)). We hypothesize that this mélange feature is a consequence of rapid calving which produces tightly packed ice, whose surface is strongly affected by fjord geometry. Three types of geometric features may be responsible: 1) the ice~~ (collapse of tightly-packed mélange~~has arched as the flow channel adjacent to the calving front is relatively narrow, limiting escape of calved ice and contributing to high compressive stress. The step change in topography is analogous to a thrust fault in bedrock subject to high compressive stresses.. 2) Bedrock-driven ice flow direction changes: ice immediately adjacent to the calving front flows along a southeast-northwest direction, while a few km downstream from the cliff, ice flow changes to a nearly east-west direction. Bedrock may be a barrier for new calved ice changing its flow direction, thereby creating a crest. 3) An underwater moraine could limit the motion of large icebergs, compressing near-field ice and contributing to the step-change. Decadal~~) events observed during the three campaigns, and corresponding changes in the ~~calving front position (Fig. 4) show that the location of the step-change coincides with the glacier terminal positions for several years since 2005. This, along with debris left by historic glacier activities, could form a moraine within the fjord. While available bed bathymetry models for Jakobshavn Isbrmædo not show such a feature, they have limited resolution, and small topographic features could be missed. The latest bed elevation model (An et al., 2017), is based on inversion of helicopter-borne gravity and radar depth sounder data, with a few depth points measured by eXpendable Current profiler (XCP) and Conductivity Temperature Depth (XCTD) probes (4 lay within the gravity survey). This model has a spatial resolution of 750 m, and an average height precision of ~60 m. Future measurements around the step-change would help to identify relevant topographic features. Additional analysis on the m~~élange~~step-change observed in the 2016 TRI data can be found in the Supplementary Text S4~~.

For both 2012 and 2015 campaigns, ~4 ~~day~~ days of data were analyzed and a 2nd-order polynomial was used to detrend the time series. For the 2016 campaign, ~13 days of data were analyzed. This time series shows significant responses to a few

~~calving~~ calving-like collapse events (Fig. ~~5~~3). We used a function composed of a 2nd-order polynomial + 3 pairs of sines and cosines to estimate the response to calving (-like) events, and then removed the polynomial. The function is:

$$V_i = a_j + b_j t + c_j t_i^2 + \sum_{k=1}^{n} [d_k \sin(2\pi f_k t_i) + e_k \cos(2\pi f_k t_i)] \quad (1)$$

where V_i is the observed LOS velocity at time t_i~~,~~, and a_j, b_j, and c_j are coefficients of 2nd-order polynomial for the jth period (nj in total), where periods are separated by ~~noticed calving~~ large calving (-like) events. To better estimate the 2nd-order polynomial, periods shorter than 1 day are not used. d_k and e_k are coefficients of the kth periodic component, with frequency f_k among those of K1/M2/S2 ~~tide constituents. After this, response~~ tidal constituents. Response to calving events and tidal constituents with periods >2 day ~~are largely eliminated~~ is largely eliminated with this procedure. Figure ~~5~~ 3 gives an example of the observed and detrended time series. Note that data in 2016 span longer times than 2012 and 2015. To save computational time, we converted TRI images into pixel sizes of 30 m × 30 m for a map-wide analysis.

Detrended time series were passed through a median filter to reduce noise. The kernel size is 3/5/5 for data in 2012/2015/2016, equal to a 9/7.5/10 minute time window. ~~After that, all~~ All time series were then analyzed using the method of Davis et al. (2014), which estimates the amplitudes and phases of the three periodic components with the same frequencies as the K1, M2 and S2 tidal constituents. This method allows us to distinguish components with close frequencies (in our case, M2 and S2). We also used a least squares fit to an equation with 3-frequencies sine/cosine as an alternative method. The two methods fit the time series equally well, with differences that are insignificant compared to noise.

Figure ~~6~~4(b,d,f) shows maps of phase lag (converted to time in h) from tidal rate to TRI observed LOS velocity at the M2 tidal frequency, along with a velocity profile for each campaign. Note that due to the phase character of periodic signals, dark red on the map represents phase values that are close to dark blue. For example, 12.42 h (period of M2) "~~equal~~equals" to 0. Note also that the phase lag maps only show pixels with signal-noise-ratio (SNR) > 1.5, where we define SNR as:

$$SNR = \frac{\sigma^2_{\text{signal}}}{\sigma^2_{\text{noise}}} \quad (2)$$

and use the root-mean-square (RMS) of the detrended velocity time series to represent σ_{signal}, and RMS of the residuals to represent σ_{noise}. We use the M2 tidal signal to illustrate tidal responses ~~in this paper~~ since this is the largest tidal constituent. Phase lag maps for K1 and S2 are shown in the Supplementary Fig. ~~S10~~S9, with patterns that are similar to M2.

Figure ~~6~~ 4 shows two types of phase lag patterns. For 2012, LOS velocity of ice in the mélange has ∼0 phase lag to tidal rate, whereas the phase lag increases sharply at the ice cliff, to ∼8.5 h on the glacier front. For both 2015 and 2016, there is a narrow zone at the glacier front that is in phase with the tidal rate, with phase lag close to 0. Upstream from that, phase lag increases to ∼8 h.

4 Discussion

4.1 Grounding line variation in a calving season

One hypothesis concerning the annual cycle of advance and retreat of Jakobshavn Isbræ is that a floating tongue grows in winter and disappears in late summer (Joughin et al., 2008; Amundson et al., 2010). However, there are no direct observations through a full calving season. We addressed this by assuming consistent behavior over the five year observation period, and considering our data to be a representative sample of early and late melt season behavior. This assumption is based on the relatively regular seasonal variations in calving front positions over the observation period from satellite images (Fig. 5), and the good inverse correlation between seasonally varying speed and length of ice tongue (Joughin et al., 2008, 2014).

Rosenau et al. (2013) looked at the cross correlation coefficient between tidal height and the vertical component of ice trajectory to estimate grounding line migration. This approach assumes that the only force that drives vertical ice motion is ~~the change of buoyancy due to~~ tide rise and fall. From an analysis of optical images, they found no evidence of floatation in mid-July 2007 (∼6 day duration), a ∼500 m wide floating zone from 8 August to 9 August 2004 (∼1 day duration), and an even wider floating zone from late spring to early summer 2010 (∼29 day duration). Podrasky et al. (2014) applied a tidal admittance model to analyze both horizontal and vertical responses to tidal forcing at Jakobshavn Isbræ. They found rapid decay of ~~admittances~~ admittance at the glacier front, corresponding to small (∼2 km and ∼0.7 km for horizontal and vertical, respectively) *e*-folding lengths (the distance over which the amplitude decreases by a factor of *e*), ~~from which they concluded~~ concluding that the glacier front was very nearly grounded in late August 2009.

TRI-derived LOS velocities reflect ~~the influence of several forcing processes~~several forcings. Surface meltwater-induced velocity variation is a quasi-diurnal signal. Podrasky et al. (2012) detected an amplitude of up to 0.1 m d^{-1} diurnal signal 20–50 km upstream from the terminus of Jakobshavn Isbræ. The timing of the diurnal maxima was ∼6 hours after local noon, ~~which corresponds~~ consistent with surface melting. Within 4 km ~~to~~ of the ice cliff, Podrasky et al. (2014) found diurnal variations that are 0.5–1 times the amplitude of tidally-forced variations, with a maxima 10.9–11.7 hours after local noon. At Helheim Glacier, Davis et al. (2014) identified a signal with peak-to-peak variation of ∼0.7 m d^{-1} in glacier flow speed at a site close to the terminus, likely associated with changes in bed lubrication due to surface melting. While surface meltwater can cause a diurnal component in ice velocity, it should have no direct influence on semi-diurnal signals, which are the dominant signals observed in all three of our campaigns. Supraglacial ~~lakes~~ lake drainage events could be another possible forcing process, though they were not observed near the terminus during our campaigns. Upstream from the terminus, supraglacial lake drainage events occur but are sporadic. Podrasky et al. (2012) observed at most three supraglacial lake drainage events near the terminus during 3 summers from 2006 to 2008. If such events occurred during our data collection periods, the responses are likely to have been eliminated by the detrending process.

The LOS velocity variation contains two components of ice motion: 1) vertical motion; 2) horizontal motion. For all three campaigns, the radar was always located higher than the ice surface in the mélange and the first ~3 km of the glacier. In this case, the TRI-observed LOS velocity ~~vertical~~ component is:

$$V_{los} = \frac{1}{\sqrt{(\frac{L}{H_0 - h})^2 + 1}} \frac{dh}{dt} \tag{3}$$

where L is the horizontal distance between ~~radar and the~~ the radar and target, H_0 is the mean height ~~of the~~ different between the radar and target, h is the vertical movement relative to H_0, and $\frac{dh}{dt}$ is the vertical component of ice velocity ~~. We presume~~ (see geometry in Supplementary Fig. S10). We assume that for floating ice, $\frac{dh}{dt}$ is correlated with the tidal rate. Hence ~~,~~ $\frac{dh}{dt} \approx$ tidal rate in the mélange, $\frac{dh}{dt}$ ~~≈ tidal rate; on~~ and less than that for the glacier, $\frac{dh}{dt}$ ~~will have a smaller range compared to tidal rate due to energy decay of tidal flexure, but the ratio~~ but can be close ~~to 1~~ if ice near the cliff is very weak, similar to what Voytenko et al. (2015a) found at the terminus of Helheim Glacier. For grounded ice, $\frac{dh}{dt}$ variation should have a much smaller amplitude compared to tidal rate variation. Horizontally, for all three campaigns, ice on almost the entire glacier moves towards the radar (LOS velocity is positive, see Supplementary Fig. S3, S4 and S5). Previous studies suggest that several mechanisms are acting simultaneously, and there is no single defined phase relation between tide variation and ice speed (e.g., Thomas, 2007; Aðalgeirsdóttir et al., 2008; Davis et al., 2014; Podrasky et al., 2014). However, at the terminus of Jakobshavn Isbræ, Podrasky et al. (2014) found that glacier speed and tidal height are anti-correlated. This likely reflects variation of back-pressure forcing associated with tide rise and fall.

We have not attempted to derive a comprehensive model for ice velocity variation caused by changes of back-pressure or other factors. Instead, we adopt the admittance parameters estimated by Podrasky et al. (2014) to assess a near-upper bound of along flow-line velocity variation. Using theodolite and GPS observations near the ice front, Podrasky et al. (2014) estimated horizontal and vertical tidal admittances of <0.12 and <0.15, respectively. In terms of phase, tide-induced vertical motion is in phase with the ocean tide, while horizontal velocity is anti-correlated with tidal height, i.e., horizontal velocity maxima are concurrent with the inflection points of tidal rate. By assuming the glacier was under the same conditions as the time when Podrasky et al. (2014) did their measurements, we predict ice velocities near the glacier front. In Fig. ~~7~~6(a), *F1* and *F2* correspond to the two points marked with purple triangles in Fig. ~~6~~4(f). For each point, two components of ice velocity were predicted and projected onto the LOS direction to the radar: 1) vertical velocity by using tidal admittance of 0.15, and time lag of 0 to tidal rate, shown by solid black curve; 2) horizontal velocity by using tidal admittance of 0.12, and anti-correlated with tidal height, shown by the dashed black curve. The red curve shows the sum of these two components. Podrasky et al. (2014) inferred that the glacier front was very ~~near~~ nearly grounded during their observation period, and both horizontal and vertical tidal admittances dropped dramatically upstream. While we use the upper bound of the tidal admittance by Podrasky et al. (2014), the amplitudes of our predicted velocities are almost the maxima for grounded ice. However, as shown in Fig. ~~7~~6(a), predicted tide-induced vertical velocities have far smaller magnitude than our TRI-derived velocities – the horizontal component is larger, but is negatively-correlated with TRI observations. Therefore, we reject the hypothesis that ice near the cliff in early summer 2016 was near grounded as during the observation period of Podrasky et al. (2014) in late

~~August~~summer. For comparison, we also plot predicted LOS velocities by assuming ice was in a free flotation state, shown in blue. This is in-phase with the TRI derived velocities, although the magnitude does not fully explain the larger signals observed by TRI. Possible reasons are discussed below.

Ice located in the low phase lag zone (dark red or blue in Fig. ~~6~~4(d)) in 2015 yields similar results. For ice further upstream in 2015 and 2016, and almost the entire glacier front of 2012, we ~~can not~~ cannot reject the possibility of a near-grounded basal condition, because the admittances by Podrasky et al. (2014) can then produce LOS velocities that are ~~sufficient~~ sufficiently large and correlated with TRI observations. Figure ~~8~~ 6(b) shows predicted (red curve) and observed ~~velocity~~ (grey dots) velocity of a surface point (*B1* in Fig. ~~6~~4(b)) that is immediately adjacent to the cliff during our 2012 campaign. ~~These two~~ They have similar amplitude and phase, though the maxima of TRI-observed velocity are not ~~explicitly~~ exactly concurrent with the inflection points of tidal rate~~, instead,~~ . Instead, they are slightly earlier (~~~~∼0.5 h) than the inflection points~~of tidal rate~~. We presume that ice in the high phase lag zone in Fig. ~~6~~ 4 is either grounded, or nearly grounded.

Based on ~~our~~ this analysis, we hypothesize that during early summer 2015 and 2016, there was a narrow zone of floating ice near the cliff, which is at least the width of the low phase lag zone (∼1 km). However, we are unable to determine if ice more than 1 km from the cliff is grounded or not. The annual maximum and minimum extents of the ice front (solid/dashed ~~pink~~ lines in Fig. ~~6) support our~~ 5) supports this hypothesis: the low phase lag zone on the glacier during both the 2015 and 2016 observations coincides with the transition zone between maximum and minimum glacier front. In contrast, for the 2012 data, the ice cliff was close to the annual minimum. Additional evidence to support this hypothesis comes from the ice surface elevation map. Figure ~~9~~ 7 shows the median average DEM from estimates of a 1 day ~~of~~ TRI measurements for each campaign. In 2012, near the centre-line of the main trough, surface ice elevation increases dramatically near the glacier front, to >140 m in <1 km distance from the cliff. In contrast, in 2015 and 2016, ice elevation increases more slowly, with a ∼1 km wide zone that is <125 m higher than local sea level. In the low elevation zone, the overall buoyancy could make ~~the condition~~ conditions favorable for a floating glacier front.

~~Figure ?? shows the annual maximum and minimum extent of Jakobshavn Isbræfrom 2012 to 2016.~~ During the time span of our TRI campaigns, the glacier front maintained a relatively ~~consistent~~ constant position, with ∼3 km ice advance and retreat per year. Time series of satellite images also suggest that in late summer to early autumn, the glacier front usually stabilizes near the minimum position for a few weeks before a steady advance. Using the TRI campaign in 2012 as a proxy for late summer conditions, and campaigns in 2015 and 2016 as proxies for early summer conditions, we infer that from 2012 to 2016, Jakobshavn Isbræ had a floating tongue in the early stage of the calving season. Under-cutting and tidal flexure then weakened the floating ice, leading to large calving events in subsequent months. During the calving season, calved ice surpassed ice flow into the terminus zone, causing the glacier front to retreat. In late stages of the calving season, the glacier had lost the majority of its floating ~~portion~~tongue, and the ice front became grounded or nearly grounded. Figure ~~??~~ 8 depicts the glacier front in early and later summer. In early summer, ice near the calving front moves in phase with tides (shown by double ~~sides~~ sided arrow in Figure ~~??a)~~8(a)).

4.2 Other sources of forcing

Figure ~~7~~ 6(a) shows that even ~~by~~ assuming ice is free-floating near the cliff, LOS velocity variation generated by tide rise and fall is insufficient to explain the observed velocity time series. Ice velocity variation caused by surface melting, if in phase with tidal rate, can increase the overall velocity variation. In this study, we did not separate the quasi-diurnal signal associated with surface melting from similar tidal components. However, there is some evidence of such a signal. As shown in ~~Fig. ??, in the low phase lag zone of 2016, if we assume diurnal along-flow-line speed variation (frequency = 1 cpd) with maxima a few h after local noon, e.g., 6 h after local noon, the related LOS velocity observed by TRI would be either correlated (when ice moves towards the radar, shown in dashed red curve) or anti-correlated (when ice moves away from the radar, shown in dashed blue curve) with LOS velocity caused by tide rise and fall. This may partly explain why the~~ the normalized PSD in Fig. 2(C)~~has less obvious diurnal constituents~~ , the diurnal constituent is less obvious compared to Fig. 2(A, B): ~~due~~ Assuming speed maxima caused by surface melting lags local noon by 6 h, it will be in phase with the K1 ocean tide rate. Due to the geometry difference, TRI-observed LOS ~~velocity is negative in box C, but positive in box A and B. The diurnal tide~~ diurnal tidal signal will be superimposed on a negative ~~or positive~~ (box C) or positive (box A and B) diurnal signal associated with surface melting, decreasing or enhancing the observed signal. Thus the diurnal constituent in Fig. 2(C) is smaller compared to the other two areas. However, surface melting should not make a significant contribution to semi-diurnal signals, as it is a ~~quasi-diurnal~~ diurnal phenomena. In addition, most sources of forcing would induce longitudinal velocity variations, and their signals should attenuate significantly near the cliff due to the LOS geometry. The large ~~extra~~ additional variation shown in Fig. ~~7~~ 6(a) has a significant transverse component, i.e., ~~along~~ in the cross flow-line direction, thus it ~~can not~~ cannot be mainly caused by surface melting~~, some other sources of forcing contribute more~~. We therefore studied points moving in a near-perpendicular direction to LOS, where along flow-line motion (e.g., velocity variation due to surface melting) is ~~trivial in~~ likely to be negligible in the TRI data. The 2016 data is appropriate for this study.

We focused on three points in the mélange ~~.~~ (Fig. 9(a)). The velocity estimates from both interferometry and feature tracking suggest that their along-flow line velocities are almost perpendicular to the radar LOS direction (within $\pm 5^\circ$ of 90°). Any longitudinal variation would be trivial when projected onto the LOS direction. Figure ~~??~~ 9 (b) shows that the LOS velocity variation caused by up-and-down ice motion that is directly related to tides can only explain about half of the observed signal. The extra signal has a strong correlation with tidal rate, with an amplitude of $\sim$1 m d^{-1} ($\sim$0.1 m in displacement). This phase relation suggests that either bed topography or tidal currents are responsible for the transverse signal. Bed topography is not likely to be the main contributor, as it is more likely to affect glacier motion rather than mélange motion, unless mélange ice is strongly attached to the glacier. There is no ocean current record during our campaigns near the glacier front, and ~~the available models are too coarse in~~ available models for the ice fjord are too coarse. However, as Doake et al. (2002) have discussed, the usually accepted drag coefficient between ice and water is not likely to create enough force to drive ice motion to a sufficient magnitude. To fully explain the periodic transverse motion of ice, we need to either assume a very rough surface for ice below the water, so that ice motion driven by tidal ~~ellipses can be~~ current is sufficient, or consider other sources of forcing. These forces are also likely to influence ice on the floating glacier tongue~~(Fig. ??).~~ . At a point on the glacier where ice moves $\sim 90^\circ$

to radar LOS (Fig. 9(c)), the TRI-derived velocity time series has a larger amplitude than the vertical tidal rate ~~.~~ (Fig. 9(d)). This suggests that the floating ice near the calving front in 2015 is weak, and moves in a ~~similar behavior as~~ manner similar to the mélange ice.

5 Conclusions

High spatial and temporal resolution measurements of the time-varying velocity field at the terminus of Jakobshavn Isbræ were acquired with ~~Terrestrial Radar Interferometry (TRI)~~terrestrial radar interferometry. Ocean tides modulate glacier velocity and this modulation can be used to infer the location of grounding line. The phase relation between ice velocity and tidal rate suggests a ∼1 km wide floating zone in early summer of 2015 and 2016, where TRI-observed velocity variation contains ice up-and-down motion caused by tide rise and fall, and perhaps transverse motion due to tidal currents. The floating zone moves together with calved ice through most of the calving season. However, in late summer 2012, there is no evidence of a floating ice tongue. We hypothesize that Jakobshavn Isbræ maintains a short floating tongue from winter to early summer, when ice flow exceeds ice loss by calving events, and the glacier front advances. In summer, iceberg calving surpasses ice flow, the glacier front retreats, and becomes nearly grounded by late summer. TRI-derived Digital Elevation Models support this hypothesis: in early summer, there is a ∼1 km wide zone with relatively thin ice (<125 m) above local sea level; in late summer, ice thickness near the cliff increases dramatically and buoyancy is insufficient to support a floating glacier front.

Competing interests. The authors declare that they have no conflict of interest.

Acknowledgements. We acknowledge Denise Holland at the Center for Global Sea Level Change in New York University for organizing the field logistics ~~in the campaign~~ for the 2015 and ~~2016.~~ 2016 campaign. Judy McIlrath of the University of South Florida is thanked for help in the 2012 fieldwork. This research was partially supported by NASA grant NNX12AK29G to T.H. Dixon. D.M. Holland acknowledges support from NYU Abu Dhabi grant G1204, NSF award ARC-1304137, and NASA Oceans Melting Greenland NNX15AD55G. S. Xie thanks Nicholas Voss at the University of South Florida for ~~the~~ helpful discussions. Landsat-7/8 and Sentinel-2 images were downloaded through the USGS EarthExplorer. ~~Envisat data were provided by the European Space Agency~~Comments from two anonymous reviewers are greatly apprieciated.

References

Aðalgeirsdóttir, G., Smith, A.M., Murray, T., King, M.A., Makinson, K., Nicholls, K.W. and Behar, A.E.: Tidal influence on Rutford Ice Stream, West Antarctica: observations of surface flow and basal processes from closely spaced GPS and passive seismic stations, J. Glaciol., 54(187), 715–724, doi:10.3189/002214308786570872, 2008.

Amundson, J.M., Fahnestock, M., Truffer, M., Brown, J., Lüthi, M.P. and Motyka, R.J.: Ice mélange dynamics and implications for terminus stability, Jakobshavn Isbræ, Greenland, J. Geophys. Res., 115(F1), doi:10.1029/2009JF001405, 2010.

An, L., Rignot, E., Elieff, S., Morlighem, M., Millan, R., Mouginot, J., Holland, D.M., Holland, D. and Paden, J.: Bed elevation of Jakobshavn Isbræ, West Greenland, from high-resolution airborne gravity and other data, Geophys. Res. Lett., 44(8), 3728–3736, doi:10.1002/2017GL073245, 2017.

Anandakrishnan, S. and Alley, R.B.: Tidal forcing of basal seismicity of ice stream C, West Antarctica, observed far inland, J. Geophys. Res., 102(B7), 15183–15196, doi:10.1029/97JB01073, 1997.

Clarke, T.S. and Echelmeyer, K.: Seismic-reflection evidence for a deep subglacial trough beneath Jakobshavns Isbræ, West Greenland, J. Glaciol., 42(141), 219–232, doi:10.1017/S0022143000004081, 1996.

Davis, J.L., De Juan, J., Nettles, M., Elosegui, P. and Andersen, M.L.: Evidence for non-tidal diurnal velocity variations of Helheim Glacier, East Greenland, J. Glaciol., 60(224), 1169–1180, doi:10.3189/2014JoG13J230, 2014.

Doake, C.S.M., Corr, H.F.J., Nicholls, K.W., Gaffikin, A., Jenkins, A., Bertiger, W.I. and King, M.A.: Tide-induced lateral movement of Brunt Ice Shelf, Antarctica, Geophys. Res. Lett., 29(8), doi:10.1029/2001GL014606, 2002.

Enderlin, E.M. and Howat, I.M.: Submarine melt rate estimates for floating termini of Greenland outlet glaciers (2000–2010), J. Glaciol., 59(213), 67–75, doi:10.3189/2013JoG12J049, 2013.

Gogineni, S., Yan, J.B., Paden, J., Leuschen, C., Li, J., Rodriguez-Morales, F., Braaten, D., Purdon, K., Wang, Z., Liu, W. and Gauch, J.: Bed topography of Jakobshavn Isbræ, Greenland, and Byrd Glacier, Antarctica, J. Glaciol., 60(223), 813–833, doi:10.3189/2014JoG14J129, 2014.

Heinert, M. and Riedel, B.: Parametric modelling of the geometrical ice-ocean interaction in the Ekstroemisen grounding zone based on short time-series, Geophys. J. Int., 169(2), 407–420, doi:10.1111/j.1365-246X.2007.03364.x, 2007.

Holland, D.M., Thomas, R.H., De Young, B., Ribergaard, M.H. and Lyberth, B.: Acceleration of Jakobshavn Isbræ triggered by warm subsurface ocean waters, Nat. Geosci., 1(10), 659–664, doi:10.1038/ngeo316, 2008.

Holland, D.M., Voytenko, D., Christianson, K., Dixon, T.H., Mel, M.J., Parizek, B.R., Vaňková, I., Walker, R.T., Walter, J.I., Nicholls, K. and Holland, D.: An Intensive Observation of Calving at Helheim Glacier, East Greenland, Oceanography, 29(4), 46–61, doi:10.5670/oceanog.2016.98, 2016.

Howat, I.M., Ahn, Y., Joughin, I., van den Broeke, M.R., Lenaerts, J. and Smith, B.: Mass balance of Greenland's three largest outlet glaciers, 2000–2010, Geophys. Res. Lett., 38(12), doi:10.1029/2011GL047565, 2011.

Iglewicz, B. and Hoaglin, D.C.: How to detect and handle outliers (Vol. 16), Asq Press, 1993.

Joughin, I., Abdalati, W. and Fahnestock, M.: Large fluctuations in speed on Greenland's Jakobshavn Isbræ glacier, Nature, 432(7017), 608–610, doi:10.1038/nature03130, 2004.

Joughin, I., Howat, I.M., Fahnestock, M., Smith, B., Krabill, W., Alley, R.B., Stern, H. and Truffer, M.: Continued evolution of Jakobshavn Isbræ following its rapid speedup, J. Geophys. Res., 113(F4), doi:10.1029/2008JF001023, 2008.

Joughin, I., Smith, B., Shean, D., and Floricioiu, D.: Brief communication: Further summer speedup of Jakobshavn Isbræ, The Cryosphere, 8, 209–214, doi:10.5194/tc-8-209-2014, 2014.

Makinson, K., King, M.A., Nicholls, K.W. and Hilmar Gudmundsson, G.: Diurnal and semidiurnal tide-induced lateral movement of Ronne Ice Shelf, Antarctica, Geophys. Res. Lett., 39(10), doi:10.1029/2012GL051636, 2012.

Motyka, R.J., Truffer, M., Fahnestock, M., Mortensen, J., Rysgaard, S. and Howat, I.: Submarine melting of the 1985 Jakobshavn Isbræ floating tongue and the triggering of the current retreat, J. Geophys. Res., 116(F1), doi:10.1029/2009JF001632, 2011.

Myers, P.G. and Ribergaard, M.H.: Warming of the polar water layer in Disko Bay and potential impact on Jakobshavn Isbræ, J. Phys. Oceanogr., 43(12), 2629–2640, doi:10.1175/JPO-D-12-051.1, 2013.

Peters, I.R., Amundson, J.M., Cassotto, R., Fahnestock, M., Darnell, K.N., Truffer, M. and Zhang, W.W.: Dynamic jamming of iceberg-choked fjords, Geophys. Res. Lett., 42(4), 1122–1129, doi:10.1002/2014GL062715, 2015.

Podrasky, D., Truffer, M., Fahnestock, M., Amundson, J.M., Cassotto, R. and Joughin, I.: Outlet glacier response to forcing over hourly to interannual timescales, Jakobshavn Isbræ, Greenland, J. Glaciol., 58(212),1212–1226, doi:10.3189/2012JoG12J065, 2012.

Podrasky, D., Truffer, M., Lüthi, M. and Fahnestock, M.: Quantifying velocity response to ocean tides and calving near the terminus of Jakobshavn Isbræ, Greenland, J. Glaciol., 60(222), 609–621, doi:10.3189/2014JoG13J130, 2014.

Richter, A., Rysgaard, S., Dietrich, R., Mortensen, J. and Petersen, D.: Coastal tides in West Greenland derived from tide gauge records, Ocean Dynamics, 61(1), 39–49, doi:10.1007/s10236-010-0341-z, 2011.

Rignot, E. and Kanagaratnam, P.: Changes in the velocity structure of the Greenland Ice Sheet, Science, 311(5763), 986–990, doi:10.1126/science.1121381, 2006.

Rignot, E., Mouginot, J. and Scheuchl, B.: Antarctic grounding line mapping from differential satellite radar interferometry, Geophys. Res. Lett., 38(10), doi:10.1029/2011GL047109, 2011.

Rosenau, R., Schwalbe, E., Maas, H.G., Baessler, M. and Dietrich, R.: Grounding line migration and high-resolution calving dynamics of Jakobshavn Isbræ, West Greenland, J. Geophys. Res., 118(2), 382–395, doi:10.1029/2012JF002515, 2013.

Rosier, S.H. and Gudmundsson, G.H.: Tidal controls on the flow of ice streams, Geophys. Res. Lett., 43(9), 4433–4440, doi:10.1002/2016GL068220, 2016.

Schoof, C.: Ice sheet grounding line dynamics: Steady states, stability, and hysteresis, J. Geophys. Res., 112(F3), doi:10.1029/2006JF000664, 2007.

Thomas, R.H.: Tide-induced perturbations of glacier velocities, Glob. Planet. Chang., 59(1), 217–224, doi:10.1016/j.gloplacha.2006.11.017, 2007.

Truffer, M. and Motyka, R.J.: Where glaciers meet water: Subaqueous melt and its relevance to glaciers in various settings, Rev. Geophys., 54(1), 220–239, doi:10.1002/2015RG000494, 2016.

Van Der Veen, C. J., Plummer, J. C. and Stearns, L. A.: Controls on the recent speed-up of Jakobshavn Isbræ, West Greenland. J. Glaciol., 57(204), 770–782, doi: 10.3189/002214311797409776, 2011.

Vieli, A., Funk, M. and Blatter, H.: Flow dynamics of tidewater glaciers: a numerical modelling approach, J. Glaciol., 47(159), 595–606, doi:10.3189/172756501781831747, 2001.

Voytenko, D., Stern, A., Holland, D.M., Dixon, T.H., Christianson, K. and Walker, R.T.: Tidally driven ice speed variation at Helheim Glacier, Greenland, observed with terrestrial radar interferometry, J. Glaciol., 61(226), 301–308, doi:10.3189/2015JoG14J173, 2015a.

Voytenko, D., Dixon, T.H., Howat, I.M., Gourmelen, N., Lembke, C., Werner, C.L., De La Peña, S. and Oddsson, B.: Multi-year observations of Breiðamerkurjökull, a marine-terminating glacier in southeastern Iceland, using terrestrial radar interferometry, J. Glaciol., 61(225), 42–54, doi:10.3189/2015JoG14J099, 2015b.

Voytenko D, Dixon T.H, Luther M.E, Lembke C, Howat I.M, de la Peña S.: Observations of inertial currents in a lagoon in southeastern Iceland using terrestrial radar interferometry and automated iceberg tracking, Comput. Geosci., 82, 23–30, doi:10.1016/j.cageo.2015.05.012, 2015c.

Voytenko, D., Dixon, T.H., Holland, D.M., Cassotto, R., Howat, I.M., Fahnestock, M.A., Truffer, M. and de la Peña, S.: Acquisition of a 3 min, two-dimensional glacier velocity field with terrestrial radar interferometry, J. Glaciol., 63(240), 629–636, doi:10.1017/jog.2017.28, 2017.

Walker, R.T., Parizek, B.R., Alley, R.B., Anandakrishnan, S., Riverman, K.L. and Christianson, K.: Ice-shelf tidal flexure and subglacial pressure variations, Earth Planet. Sci. Lett., 361, 422–428, doi:10.1016/j.epsl.2012.11.008, 2013.

Walters, R.A.: Small-amplitude, short-period variations in the speed of a tide-water glacier in south-central Alaska, USA, Ann. Glaciol., 12, 187–191, doi:10.1017/S0260305500007175, 1989.

Werner, C., Strozzi, T., Wiesmann, A. and Wegmüller, U.: GAMMA's portable radar interferometer, In Proc. 13th FIG Symp. Deform. Meas. Anal, 1–10, 2008.

Xie, S., Dixon, T.H., Voytenko, D., Holland, D.M., Holland, D. and Zheng, T.: Precursor motion to iceberg calving at Jakobshavn Isbræ, Greenland, observed with terrestrial radar interferometry, J. Glaciol., 62(236), 1134–1142, doi:10.1017/jog.2016.104, 2016.

Table 1. ~~Parameters used for~~ TRI ~~measurements~~observation parameters

Year	Start day	End day	Scanned arc (°)	Repeat time* (min)
2012	31 July	12 August	120	3
2015	6 June	10 June	150	1.5
2016	7 June	20 June	170	2

∗ Time between two adjacent scans.

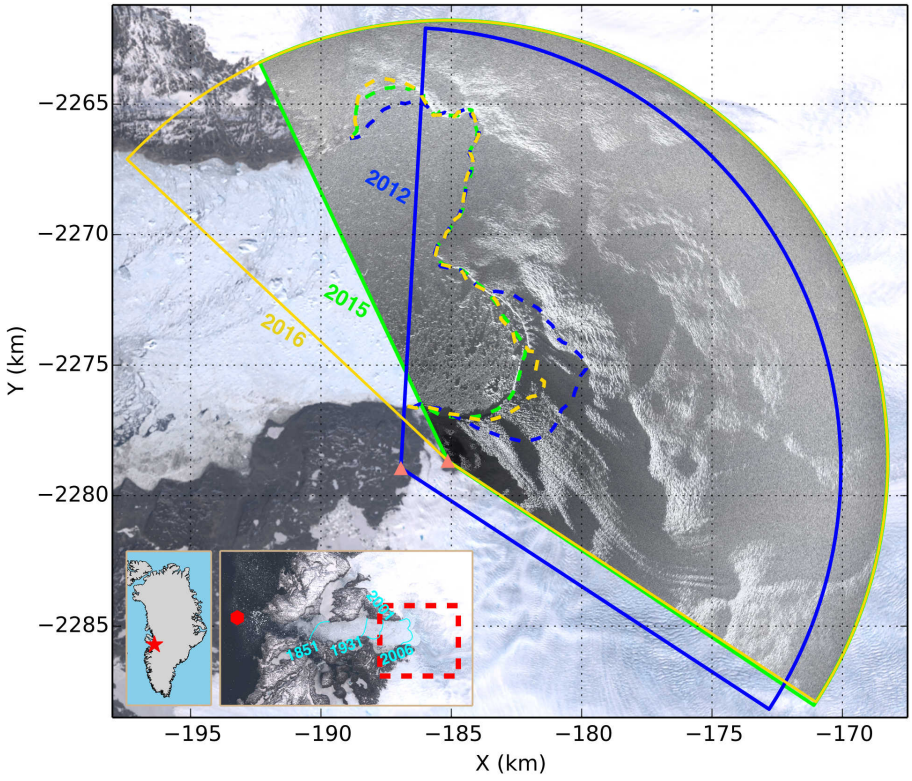

Figure 1. TRI scan areas in 2012 (blue), 2015 (green) and 2016 (yellow). An intensity image of radar backscatter from the 2015 campaign (acquired 9 June 2015) is overlain on a Landsat-8 image (acquired 4 June 2015). Dashed lines indicate ice cliff locations derived from satellite images: Landsat-7 on 6 August for 2012; Landsat-8 on 4 June for 2015; and Landsat-8 on 13 June for 2016. Triangles in salmon color show locations of the radar. Dashed red box in the insert outlines the area shown in the main figure. Cyan lines in the insert show the calving front positions in different years, courtesy of NASA Earth Observatory (https://earthobservatory.nasa.gov/Features/Greenland/greenland3.php). Red hexagon marks the mooring location where tidal height was recorded in 2015. Red star shows the location of the study area in Greenland. Coordinates are in polar stereographic projection, corresponding to EPSG: 3413.

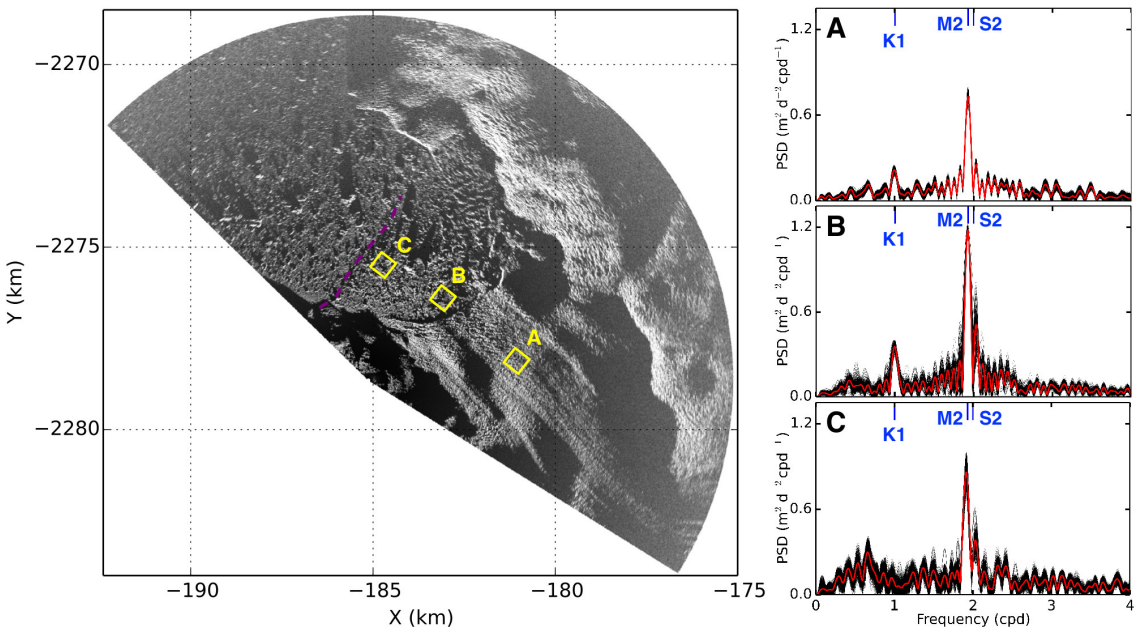

Figure 2. Stacked power spectral density (PSD) estimates of the LOS velocity time series for selected areas in 2016. Three 0.5 km × 0.5 km boxes (A, B, and C) mark the selected areas. PSD plots are normalized, and each black line represents 1 pixel (10 m × 10 m) in the corresponding box. Red line shows mean value. Blue lines mark frequencies of K1, M2, and S2 tide constituents. On map at left, dashed purple line shows a significant step-change of height in the mélange observed in 2016 (see also in Fig. 3(a)).

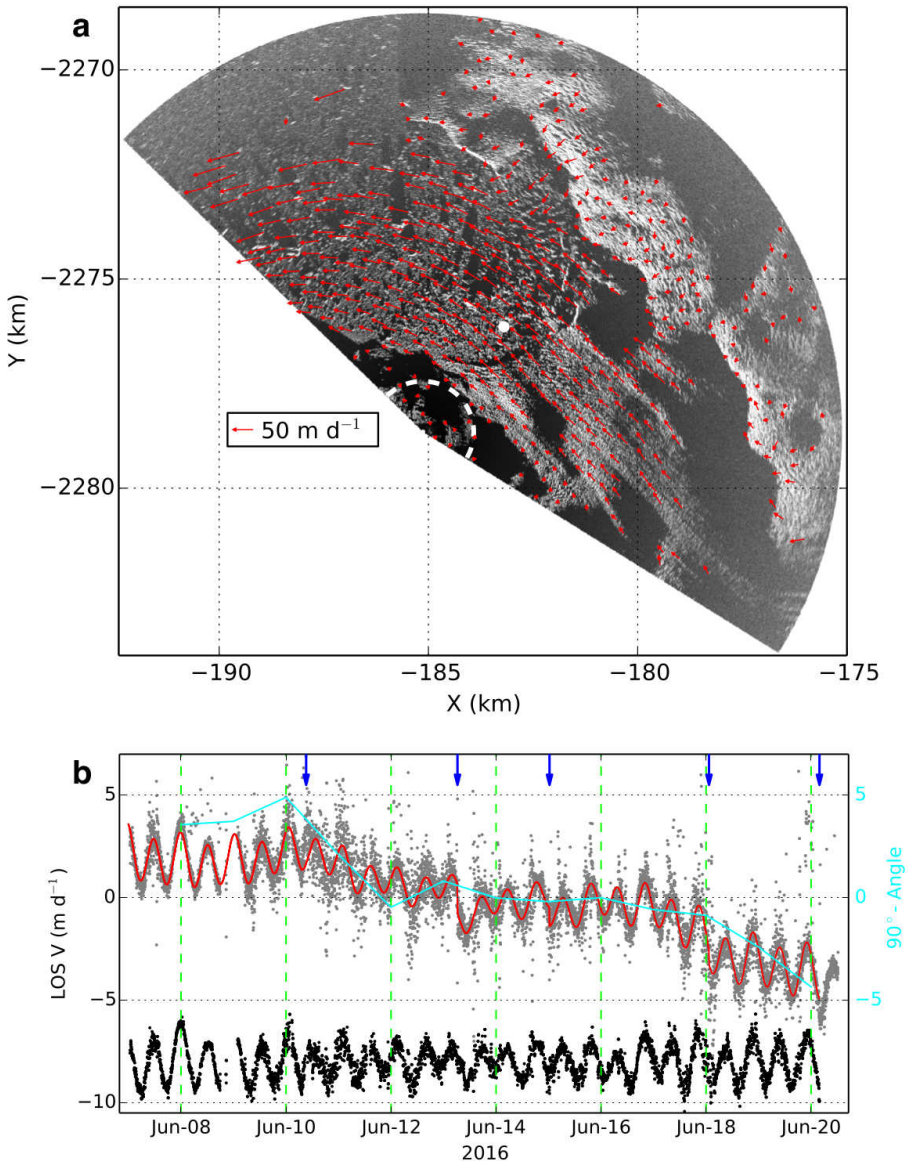

Figure 3. (a) Ice velocity estimated by feature tracking using a pair of TRI intensity images separated by one day in 2016 campaign. Dashed outlines the area with (near-) stationary points used to define uncertainty of velocity estimate (RMS <1 m d^{-1}). (b) TRI observed LOS velocity time series for a single point, marked by white dot in (a). Grey dots show velocities derived from unwrapped phases, red curve shows the model used to remove perturbations caused by calving events, black dots show detrended time series offset by -8 m d^{-1}. Blue arrows mark large calving or calving-like collapse events. Cyan line shows changes of angle between LOS and 2-D ice velocity direction by feature tracking. The LOS velocity variation for period longer than 1 d is mostly due to changes in background velocity direction.

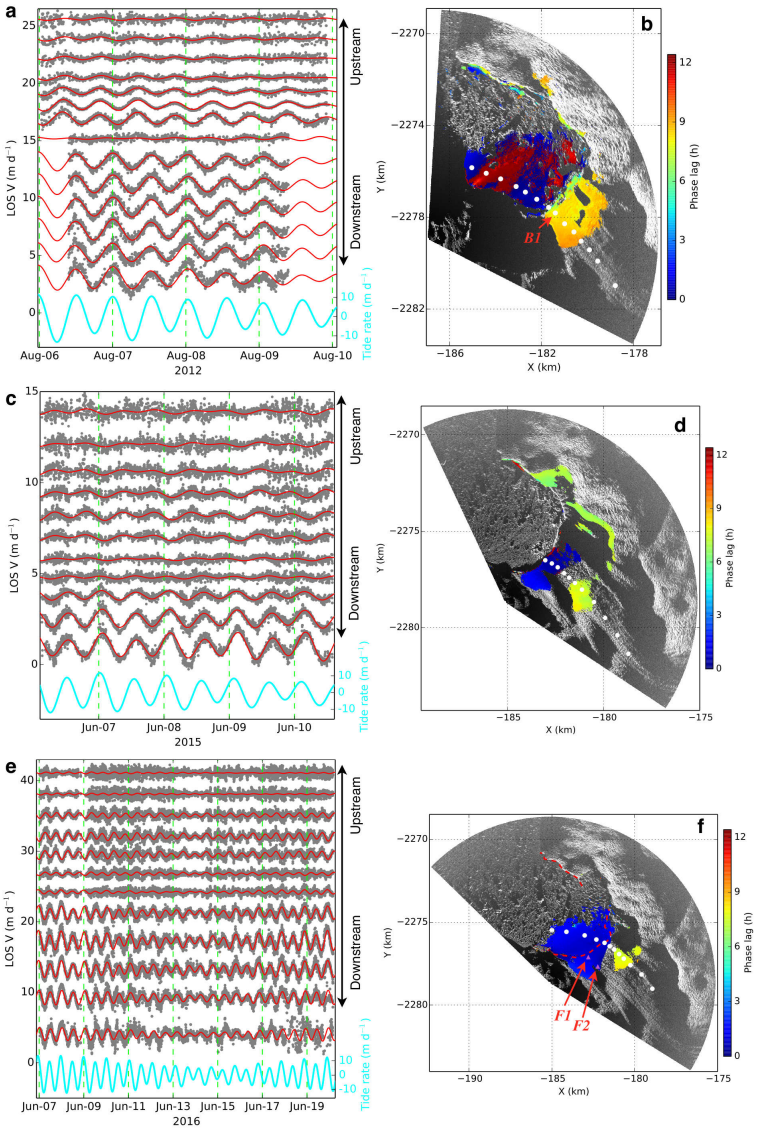

Figure 4. Phase lag map and velocity time series for a profile in each campaign. Grey dots (a, c, e) show detrended LOS velocity time series for a profile along the ice flow-line, marked by white dots on the map at right. Red curve shows best model fit. LOS velocities are offset for clarity. Cyan curve shows tidal rate. Phase lag map (b, d, f) show M2 frequency signal. Areas where SNR<1.5 are omitted. Phase lags are converted to times (in h). In (f), dashed red line shows TRI derived location of ice cliff on 13 June 2016. Note that the amplitude of detrended LOS velocity depends on a number of factors, including tidal response, ice flow direction relative to radar LOS, distance up-glacier, whether the scanned area is glacier or mélange, and (within the mélange) whether the imaged pixel is close to or far from the calving front.

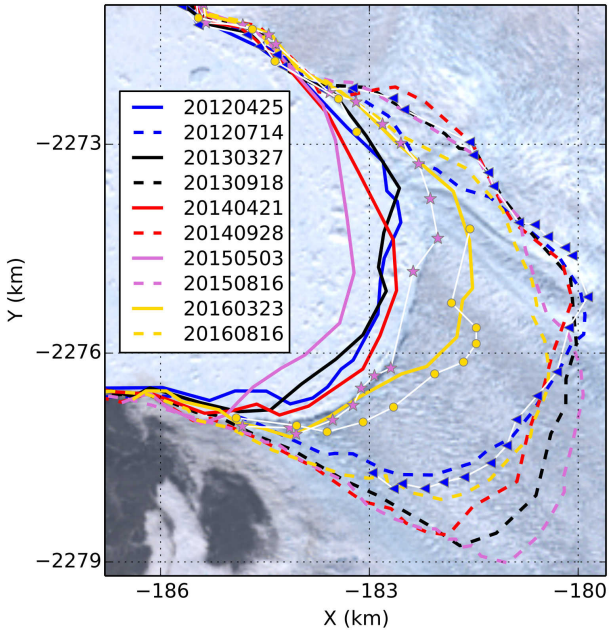

Figure 5. Annual maximum and minimum extents of Jakobshavn Isbræ's calving front from 2012 to 2016. Solid lines show the ice cliff when glacier extent is maximum, dashed lines when glacier extent is minimum. Ice cliff locations are derived from available Landsat-7/8 and Sentinel-2 images in USGS archive. Legends are dates of image acquisition. Lines with triangles, stars and circles show ice cliff locations during TRI campaigns in 2012 (6 August), 2015 (9 June) and 2016 (13 June), respectively. Background for this figure is a Landsat-8 image acquired on 4 June 2015.

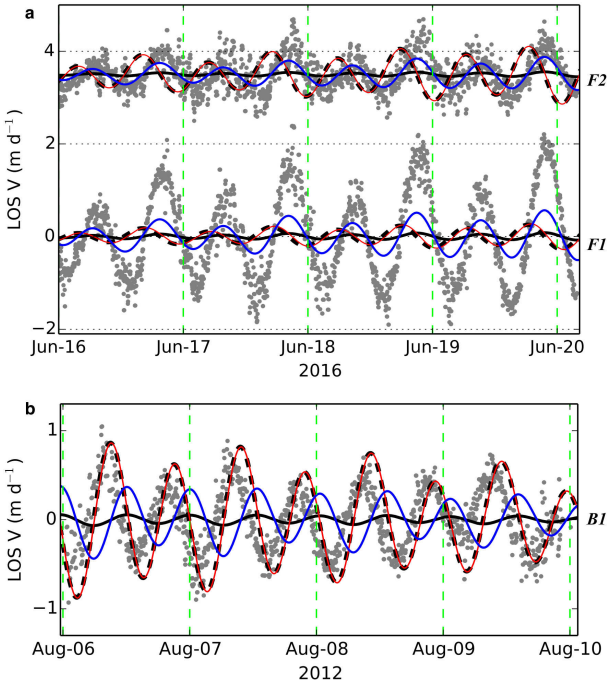

Figure 6. (a) Detrended LOS velocities of points located in the low phase lag zone in 2016. *F1* and *F2* are the two points marked with purple triangles in Fig. 4(f), *F2* (upstream one) has been offset by 3.5 m d^{-1} for clarity. Grey dots are observed time series. Solid black curve shows vertical response to tide variations, using admittance of 0.15 (Podrasky et al., 2014) projected onto the LOS direction. Dashed black curve is horizontal response by using admittance of 0.12, projected onto the LOS direction. Red curve shows the sum of solid and dashed black curves, its Pearson correlation coefficient with observed time series is -0.13 and -0.19 for *F1* and *F2*, respectively. Blue curve shows predicted LOS velocity by assuming ice is free floating; its Pearson correlation coefficient with observed time series is 0.82 and 0.69 for *F1* and *F2*, respectively. Note that ∼4 days of data are used in this figure for clarity. (b) LOS velocities of a point immediately adjacent to the ice cliff in 2012 (*B1* in Fig. 4(b)), colors and curves represent the same parameters as in (a). The Pearson correlation coefficient with observed time series is 0.65 for the red curve (grounded or nearly grounded assumption, the same as Podrasky et al. (2014)), and -0.56 for the blue curve (free floating assumption).

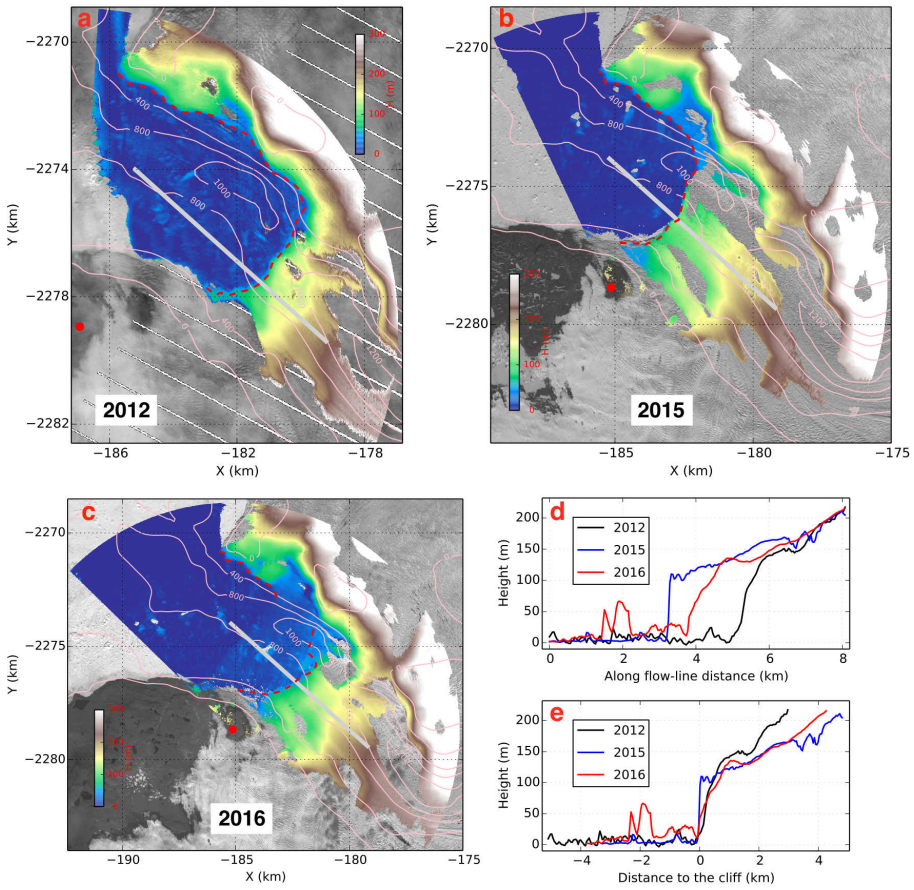

Figure 7. DEM for the glacier front, derived from median average of DEM estimates separated by 2 minutes during a 1 day period. For each subplot, red dot shows location of the radar, pink contours show bed bathymetry (An et al., 2017). Dashed red line shows the ice cliff from TRI image, note that in 2016 it was not possible to distinguish a portion of the ice cliff from TRI measurements, hence it is not marked on the map. The background image for (a) was acquired on 6 Aug 2012 by Landsat-7, white stripes are data gaps. Background image in (b) was acquired on 4 Jun 2015 by Landsat-8. Background image in (c) was acquired on 13 Jun 2016 by Landsat-8. Note that uncertainty increases with distance to the radar. Black, blue, and red line in (d) show elevation profiles along a transect marked (grey lines in a–c). These transects have the same location in space. In (e), the distance of each transect is normalized so that the cliffs are in the same position.

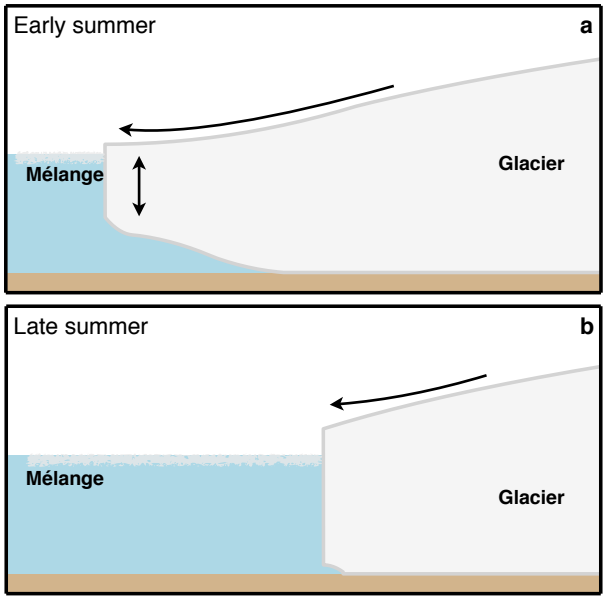

Figure 8. Cartoon of glacier front in early (a) and late (b) summer. Ice shown in light grey, water shown in light blue, bed shown in brown. Single-sided arrow indicates direction of glacier flow. Double sided arrow in (a) indicates that ice tongue moves in phase with tides. Note that the ice cliff is higher in late summer than early summer.

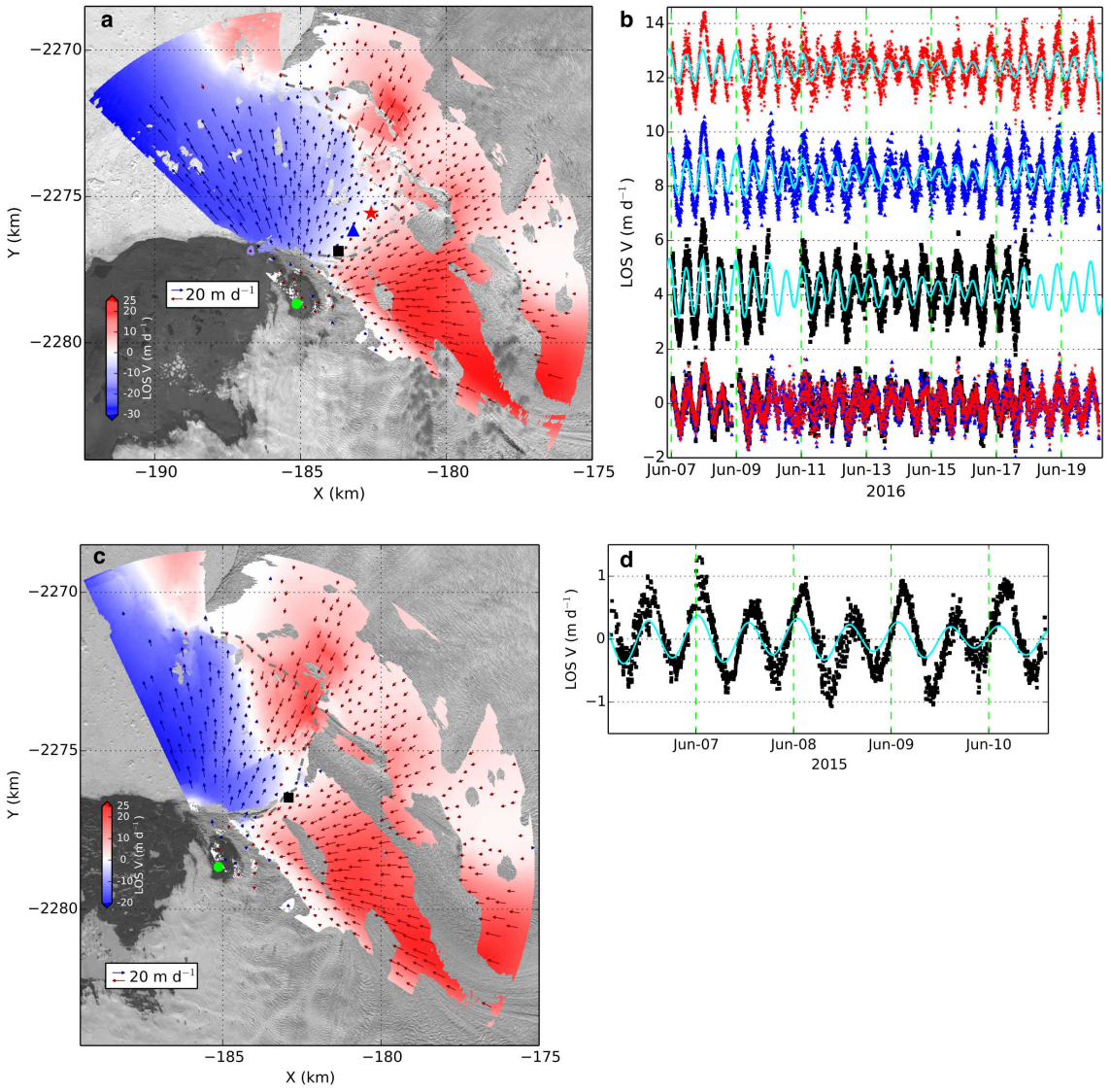

Figure 9. (a, b) Transverse ice motion in the mélange of 2016. In (a), color map shows LOS velocity by interferometry, from a 1 day median average. Arrows show velocity estimates from feature tracking projected onto the LOS direction (dark red when ice moves towards the radar and dark blue when ice moves away). Dashed grey line shows cliff location from TRI image. black square, blue triangle and red star mark three points where 2-D velocity direction is nearly perpendicular to radar LOS. Their LOS velocity time series are shown in (b). Note that the point with blue triangle marker corresponds to the marked point in Fig. 3(a). Top 3 rows in (b) show TRI observed LOS velocities for selected points; cyan curves are predicted LOS velocities based on the imaging geometry, assuming ice is free floating. LOS velocities are offset for clarity. Bottom row shows residual time series by subtracting the cyan curves. (c, d) Transverse ice motion on the glacier front for 2015. Colors and arrows in (c) represent the same parameters as in (a). A point immediately adjacent to the cliff was chosen, marked by black square with its LOS velocity observed with TRI and predicted by tide variations shown in (d). Cyan curve in (d) shows predicted LOS velocities.